2MASS 0213+3648 C: a wide T3 benchmark companion to an active, old M dwarf binary

N. R. Deacon,[1,2]* E. A. Magnier,[3] Michael C. Liu,[3]† Joshua E. Schlieder,[2,4]
Kimberly M. Aller,[3] William M. J. Best,[3] Brendan P. Bowler,[5]‡ W. S. Burgett,[6]
K. C. Chambers,[3] P. W. Draper,[7] H. Flewelling,[3] K. W. Hodapp,[8] N. Kaiser,[3]
N. Metcalfe,[7] W. E. Sweeney,[3] R. J. Wainscoat[3] and C. Waters[3]

[1]*Centre for Astrophysics Research, University of Hertfordshire, College Lane, Hatfield AL10 9AB, UK*
[2]*Max Planck Institute for Astronomy, Konigstuhl 17, Heidelberg D-69117, Germany*
[3]*Institute for Astronomy, University of Hawaii at Manoa, 2680 Woodlawn Drive, Honolulu, HI 96822, USA*
[4]*NASA Postdoctoral Program Fellow, NASA Ames Research Center, Moffett Field, CA, USA*
[5]*Department of Astronomy, The University of Texas at Austin, 2515 Speedway, Austin, TX 78712, USA*
[6]*Giant Magellan Telescope Observatory, USA*
[7]*Department of Physics, University of Durham, South Road, Durham DH1 3LE, UK*
[8]*Institute for Astronomy, University of Hawai'i, 640 North Aohoku Place, Hilo, HI 96720, USA*

ABSTRACT

We present the discovery of a 360 au separation T3 companion to the tight (3.1 au) M4.5+M6.5 binary 2MASS J02132062+3648506. This companion was identified using Pan-STARRS 1 data and despite its relative proximity to the Sun ($22.2^{+6.4}_{-4.0}$ pc; Pan-STARRS 1 parallax) and brightness ($J = 15.3$), it appears to have been missed by previous studies due to its position near a diffraction spike in 2MASS. The close M dwarf binary has active X-ray and Hα emission and shows evidence for UV flares. The binary's weak *GALEX* UV emission and strong Na I 8200 Å Na absorption lead us to an age range of ∼1–10 Gyr. Applying this age range to evolutionary models implies that the wide companion has a mass of 0.063 ± 0.009 M$_\odot$. 2MASS J0213+3648 C provides a relatively old benchmark close to the L/T transition and acts as a key, older comparison to the much younger early-T companions HN Peg B and GU Psc b.

Key words: binaries: visual – brown dwarfs – stars: low-mass.

1 INTRODUCTION

Wide multiple systems are common in the solar neighbourhood, with >25 per cent of solar-type stars having a companion wider that 100 au (Raghavan et al. 2010). However, the formation mechanism of these systems, especially those wider than ∼5000 au, presents a challenge for models of star and brown dwarf formation. Current suggestions are that such companions formed *in situ* were captured in their birth cluster (Kouwenhoven et al. 2010) or result from the evolution of higher order multiple systems (Delgado-Donate et al. 2004; Umbreit et al. 2005; Reipurth & Mikkola 2012). This last theory predicts that wide binaries originate in tertiary systems

and that dynamical interactions can drive these systems into being a close binary pair with a wider companion. Thus, wide binary components should have a large, higher order multiplicity fraction [as seen in the literature review of substellar objects by Burgasser, Kirkpatrick & Lowrance (2005) and observed for M dwarfs by Law et al. (2010)] and that wide companions to close binaries should be more common than wide companions to single stars [seen by Allen et al. (2012)].

Wide substellar companions, in particular, are also useful as test beds for evolutionary and atmospheric models. Such objects fall into two categories, 'mass benchmarks' (Liu, Dupuy & Ireland 2008) where two of the system components are close enough to have an orbit that can be measured and thereby yield a dynamical mass, and 'age benchmarks', where the age of the primary is determined (typically from activity or rotation) and then applied to the secondary. Rare systems that are both age and mass benchmarks have both a higher mass primary for age determination and low-mass object with dynamical mass measurements (Dupuy, Liu & Ireland 2009; Crepp et al. 2012; Dupuy, Liu & Ireland 2014).

* E-mail: n.deacon2@herts.ac.uk

† Visiting Astronomer at the Infrared Telescope Facility, which is operated by the University of Hawaii under Cooperative Agreement no. NNX-08AE38A with the National Aeronautics, Space Administration, Science Mission Directorate, Planetary Astronomy Program.
‡ McDonald Prize Fellow.

The past decade has seen an explosion in the discovery of wide ultracool[1] companions to stars and brown dwarfs. Reviews of this population are presented in Faherty et al. (2010) and Deacon et al. (2014). Currently, there are 22 known T dwarf companions with separations greater than 100 au, the 21 listed in the literature review of Deacon et al. (2014) plus the recently discovered companion to the exoplanet host star HIP 70849 (Lodieu et al. 2014). Of these, four (Gl 570 D, Burgasser et al. 2000; Wolf 1130 B, Mace et al. 2013; Ross 458 C, Goldman et al. 2010, and ξ UMa E, Wright et al. 2013) lie in systems with higher order stellar multiplicity. Relatively few known T dwarfs companions lie in young systems. HN Peg B is a T2.5 (Luhman et al. 2007) companion to a ∼300 Myr G0 dwarf. It is well fitted by the spectral standards with only a possibly weaker 1.25-µm potassium doublet hinting at reduced gravity. By contrast, the younger (∼100 Myr), lower mass T3.5 GU Psc b (Naud et al. 2014) diverges significantly from the spectral standards in the *Y*, *J* and *K* bands. Naud et al. (2014) suggest that this may be due to a differing amount of collision-induced absorption from molecular hydrogen or possibly due to an unresolved, cooler companion. These are the only T2.5–3.5 companions in the literature.

Here we present a wide separation T3 companion to a known, active M dwarf binary system in the solar neighbourhood discovered during our search for ultracool companions using Pan-STARRS 1.

2 OBSERVATIONS

2.1 Identification in Pan-STARRS 1 data

The Pan-STARRS 1 telescope (Kaiser et al. 2002; Chambers et al. 2016) is a wide-field 1.8-m telescope on Haleakala on Maui in the Hawaiian Islands and has recently completed its 3.5-yr science mission. Pan-STARRS 1 data are reduced and calibrated photometrically and astrometrically by a process described by Magnier (2006, 2007), Magnier et al. (2013, 2016), and Schlafly et al. (2012). The telescope undertook a series of sky surveys including the 3π Survey, covering 30 000 deg² north of δ = −30° with two pairs of observations per year in each of five filters. These filters (g_{P1}, r_{P1}, i_{P1}, z_{P1} and y_{P1}; Tonry et al. 2012) extend further into the red optical than SDSS, making Pan-STARRS 1 appealing for studying late-type objects in the solar neighbourhood (Deacon et al. 2011; Liu et al. 2011, 2013; Best et al. 2013, 2015). This combination of properties has already resulted in the identification of the largest number of ultracool companions to date, with a near-doubling of the late-M and L dwarf wide separation (>100 au) companion populations (Deacon et al. 2014) as well as the discovery of two T dwarf companions (Deacon et al. 2012a,b).

We searched the 3π data set processed by the first version of the Pan-STARRS 1 pipeline to be run on the full survey area (aka. PV1) for wide companions to nearby stars. As in Deacon et al. (2014), we included objects from various proper motion catalogues, but unlike this previous work, we did not exclude nearby objects with low proper motion (<0.1 arcsec yr⁻¹). We followed the same selection process as Deacon et al. (2014) selecting only objects with proper motions measured over a >400-d baseline, requiring a 5σ overall significance and two individual detections in y_{P1}. This process included checking the 2MASS Reject Table as well as the main 2MASS data base for near-infrared data. One candidate we identified was an apparent companion to a mid-M dwarf at ∼15 pc

2MASS J02132062+3648506 (aka PSO J33.3327+36.8105; hereafter 2MASS J0213+3648). This object came into our input primary list from the nearby M dwarf catalogue of Lépine & Gaidos (2011). 2MASS J0213+3648 was discovered as an M4.5 by Riaz, Gizis & Harvin (2006) and identified as a close (0.217 arcsec) binary by Janson et al. (2012), we refer to the unresolved M dwarf binary as 2MASS J0213+3648 AB. From the contrast ratio (Δ*i* = 2.16 ± 0.15 mag), Janson et al. (2012) estimated a spectral type of M6.5 for the secondary component with the primary remaining an M4.5. The primary+secondary pair is saturated and unresolved in Pan-STARRS 1 imaging. Our candidate common proper motion companion showed contaminated 2MASS photometry (flagged as c for confusion) from a nearby diffraction spike and did not appear in the survey data taken by the Wide-field Infrared Survey Explorer (WISE; Wright et al. 2010), neither in the main All-WISE table nor in the All-WISE Reject Table (Cutri et al. 2013). This may be due to the proximity of two bright stars (including the primary) within half an arcminute. The flagged 2MASS detection and WISE non-detection are the likely reasons for this otherwise bright, nearby T dwarf remaining undiscovered until now. Fig. 1 shows the companion in a number of different Pan-STARRS 1, 2MASS, and WISE filters.

2.1.1 Probability of chance alignment

In order to estimate if our proposed companion and its primary are due to a chance alignment between unrelated objects, we used a modified version of the test presented in Lépine & Bongiorno (2007). In the original test, the positions in the input primary catalogue are offset by several degrees before the pairing between the primaries and with potential secondaries is carried out. This means the resulting data should contain only coincidental pairings. The pairings are then plotted on a proper motion difference versus separation plot with a maximum separation of 10 arcmin. Here, we take a slightly different approach as we also have a trigonometric parallax for the companion (Section 2.5). Hence, we assign a quantity that we call the 'astrometric offset'. This is a quadrature sum of the proper motion differences in each axis and the parallax difference, each divided by the error on that quantity. Hence,

$$n_\sigma^2 = \frac{(\mu_{\alpha1} - \mu_{\alpha2})^2}{(\sigma_{\mu\alpha1}^2 + \sigma_{\mu\alpha2}^2)} + \frac{(\mu_{\delta1} - \mu_{\delta2})^2}{(\sigma_{\mu\delta1}^2 + \sigma_{\mu\delta2}^2)} + \frac{(\pi_1 - \pi_2)^2}{(\sigma_{\pi1}^2 + \sigma_{\pi2}^2)}. \quad (1)$$

We drew primaries with measured photometric distances within 20 pc from the list of 8889 (7464 within the Pan-STARRS 1 survey area) bright M dwarfs presented in Lépine & Gaidos (2011). These photometric parallaxes were used in the calculation of the astrometric offset. No lower proper motion limit was set on top of the 40 mas yr⁻¹ lower limit in our input primary list. We then offset the positions of these object by two degrees in Right Ascension and carried out a pairing process with late-type ($z_{P1} - y_{P1} > 0.8$) objects in the Pan-STARRS 1 data base. We made a conservative cut on the χ_ν^2 (the χ^2 per degree of freedom) statistic of the astrometric points around the Pan-STARRS 1 data base parallax fit limiting it to be <10 and limited ourselves to objects detected in eight or more Pan-STARRS 1 images [this latter cut is identical to one used in Deacon et al. (2014)]. The astrometry used for our pair was the proper motion and the photometric parallax for the primary from Lépine & Gaidos (2011) and our own proper motion and parallax for the secondary (calculated in Section 2.5). Our results are shown in Fig. 2, with plots showing n_σ both with and without the parallax term. Clearly, the pairing of 2MASS J0213+3648 AB with our proposed companion is distinct from the coincident

---

[1] Objects with spectral types M7 or later.
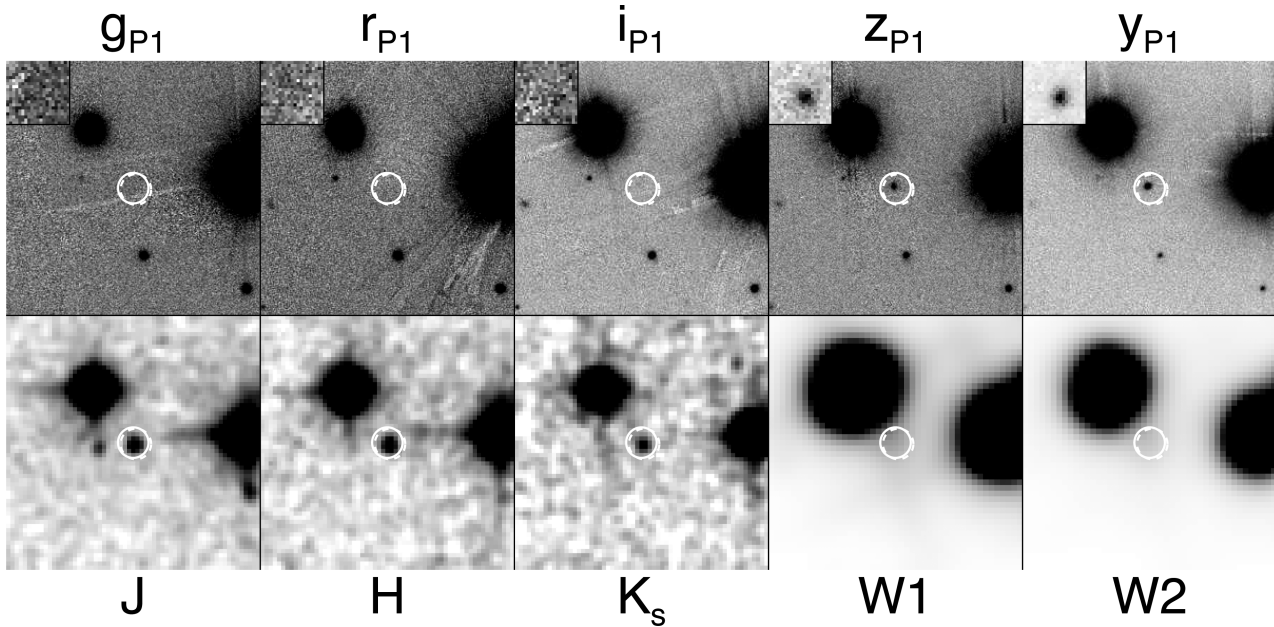
Figure 1. Discovery images of the wide T companion (centre) and its bright primary (to the North and East of the companion). Each image is 60 arcsec across with North up and East left. The small cutouts in the PS1 images are 10 arcsec across centred on the companion. Note that the object is not detected in *W*1 and *W*2 possibly due to contamination from nearby bright stars. The solid circle marks the 2010.0 position and the dashed circle the 2MASS position. The PS1 image is a stack of images taken over the duration of the survey (2010–2013), so the object will not fall exactly at the 2010.0 position and may appear smeared due to proper motion.

pairing locus. As there are no stars in our coincident pairing test with similar distances and astrometric offsets to 2MASS J0213+3648, we are unable to calculate a formal chance alignment probability. The inclusion of parallax data also significantly reduces the number of chance alignment pairings.

2.2 UK Infrared Telescope photometry

As the photometry from 2MASS was strongly affected by a diffraction spike, we obtained UKIRT/WFCAM (Casali et al. 2007) observations of 2MASS J0213+3648 C on UT 2015 July 31. These observations were reduced using the WFCAM reduction pipeline (Irwin et al. 2004; Hodgkin et al. 2009) by the Cambridge Astronomical Survey Unit. The resulting photometry is in Table 1.

2.3 NASA Infrared Telescope Facility spectroscopy

Our candidate companion was observed on UT 2015 October 5, with the recently upgraded SpeX spectrograph (Rayner et al. 2003) on the NASA Infrared Telescope Facility. Conditions were non-photometric with periods of high humidity and seeing of 0.6–1.0 arcsec. The observation was made at an airmass of 1.06 with three pairs of 50 s observations nodded in an ABBA pattern. The low-resolution prism mode was used along with the 0.8 arcsec slit giving a spectral resolution of $R = 75$, with the slit aligned to the parallactic angle to minimize slit losses due to atmospheric dispersion. An A0V standard star (HD 22859) was observed contemporaneously at a similar airmass to the target. The spectrum was reduced using version 4.0 of the SPEXTOOL software package (Cushing, Vacca & Rayner 2004; Vacca, Cushing & Rayner 2003). The final spectrum for 2MASS J0213+3648 C is shown in Fig. 9 and the analysis of this spectrum is discussed in Section 3.2.

The unresolved primary 2MASS J0213+3648 A/B was observed on UT 2015 September 25 with SpeX. Conditions were mostly clear

with seeing of 0.5−0.8 arcsec. The 0.3 arcsec slit was used along with the cross-dispersed SXD mode yielding a spectral resolution of $R = 2000$. The observation was made at an airmass of 1.05 and consisted of four pairs of 14.8 s observations nodded in an ABBA pattern. The reduction technique described above for the companion was also used but with the comparison star HD 19600. The spectrum is shown in Fig. 3. We discuss the use of the 8200 Å Sodium doublet in this spectrum in Section 3.1.1.

2.4 Calar Alto 2.2 m spectroscopy

2MASS J0213+3648 AB was observed under poor conditions on 2014 November 11 UT using the Calar Alto Fibre-Fed Echelle spectrograph (CAFE; Aceituno et al. 2013) on the 2.2-m telescope at Calar Alto Observatory in Almeria, Spain. A single 750 s exposure was obtained under clear skies with high, variable humidity and poor seeing (>2 arcsec). Along with the science target, two radial velocity standards from Nidever et al. (2002) were observed for internal calibration checks, GJ 908 and HD 26794. Both standards were observed under slightly better conditions with single exposures of 400 s and 800 s, respectively. We also obtained a set of calibration observations prior to 2MASS J0213+3648 AB and the standards that included bias frames, continuum lamp flats and ThAr lamp frames for wavelength calibration. The data were reduced using the observatory pipeline described in Aceituno et al. (2013), which bias corrects, flat-fields and wavelength calibrates the data and applies a rough flux calibration.

The reduced spectrum of 2MASS J0213+3648 AB has a signal-to-noise ratio (SNR) of ∼3 per pixel, the RV standards have SNRs of ∼25. To measure our target's radial velocity, we selected a region of the spectrum spanning 6600–6640 Å that was relatively free of telluric lines, had some strong stellar absorption lines, and was in the part of the spectrum with the highest SNR. This 40 Å region was
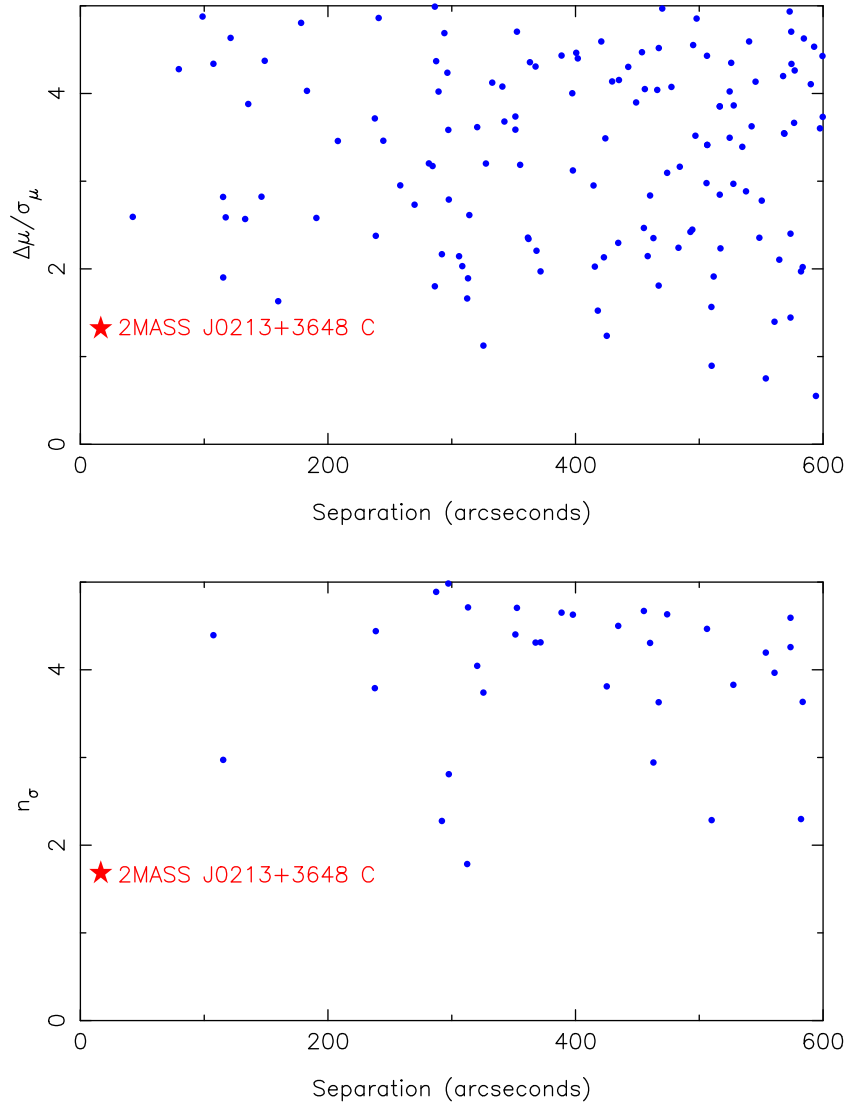
Figure 2. Comparing our companion with a sample coincident pairings generated by searching for late-type ($z_{P1} - y_{P1} > 0.8$ companions around all M dwarfs in the catalogue of Lépine & Gaidos (2011) with photometric distances within 20 pc. The positions of these M dwarfs were offset by two degrees so only coincident pairings (blue dots) should be included. top: the *y*-axis shows the quadrature sum of the difference in proper motion between each pair in terms of the number of standard deviations Bottom: the *y*-axis shows the quadrature sum of the differences in proper motion and parallax between each pair in terms of the number of standard deviations. The inclusion of parallax data clearly reduces the contamination from background stars.

flattened by dividing by the continuum polynomial fit and reduced from a resolution of ∼65 000 to ∼48 000 by convolving with a Gaussian kernel. This last step was taken to match the resolution of the late-type RV templates used for cross-correlation (CC) observed using FEROS on the ESO/MPG 2.2 m telescope at La Silla. A barycentric velocity correction was also applied to the CAFE spectra. Our initial radial velocities for our RV standards were discrepant from the values in Nidever et al. (2002) by −58 km s^{-1}. We were unable to find the source of this discrepancy so can only correct for it post hoc. This results in values of −71.8 ± 1.0 km s^{-1} compared to the literature value of −71.3 ± 0.1 km s^{-1} for GJ 908 and 57.0 ± 1.0 km s^{-1} compared to 56.6 ± 0.1 km s^{-1} for HD 26794. This process and correction yielded a radial velocity of 1.5 ± 1.4 km s^{-1} for 2MASS J0213+3648 AB although the low SNR meant that the cross-correlation power has a poor value of 20 per cent. The error in the radial velocity is the quadrature sum of the measured error on a Gaussian fit to the cross-correlation peak

and a systematic error of 1 km s^{-1} introduced by the use of the observed RV templates. There is also the additional factor of the RV amplitude induced by the secondary, which is approximately 2 km s^{-1}.

2.5 Pan-STARRS 1 astrometry

Pan-STARRS 1 has observed each field in the 3π survey repeatedly over several years, allowing us to measure the parallax and proper motions of 2MASS J0213+3648 C. We were unable to calculate a parallax or proper motion for 2MASS J0213+3648 AB due to saturation. The Pan-STARRS 1 astrometric analysis of 2MASS J0213+3648 C consists of an initial series of transformations to remove distortions caused by the Pan-STARRS 1 optical system and camera. An iterative astrometric correction process is then used to determine the conversion from chip to celestial coordinates, minimizing the scatter between object positions on

Table 1. The properties of the components of the 2MASS J02132062+3648506 system. Note that we do not quote Pan-STARRS 1 magnitudes for 2MASS J0213+3648 AB as it is heavily saturated.

| | 2MASS J0213+3648 AB | | |
	2MASS J0213+3648 A	2MASS J0213+3648 B	2MASS J0213+3648 C
Position	02 13 20.63 +36 48 50.7[a]		02 13 19.82 +36 48 37.5[a]
μ^α (arcsec yr^{-1})	0.024 ± 0.008[e]		0.024 ± 0.010
μ^δ (arcsec yr^{-1})	0.047 ± 0.008[e]		0.065 ± 0.011
π (arcsec)	0.068 ± 0.020[e,*]		0.045 ± 0.010[f]
			$0.063^{+0.014}_{-0.010}$[f,*]
Separation	0.217″[b]		16.4″[a]
	4.8 AU[f]		360 AU[f]
Spectral Type	M4.5[c]		T3
	M4.5[d]	M6.5[d]	
V (mag)	13.86[e]		–
Δi (mag)	–	2.16 ± 0.15[g]	
Δz (mag)	–	2.42 ± 0.18[g]	
z_{P1} (AB mag)	–		19.243 ± 0.016[f]
y_{P1} (AB mag)	–		17.567 ± 0.010[f]
J_{2MASS}	9.367 ± 0.022[a]		15.297 ± 0.53[a,†]
H_{2MASS}	8.825 ± 0.021[a]		14.765 ± 0.62[a,‡]
$K_{s, 2MASS}$	8.518 ± 0.018[a]		14.770 ± 0.115[a,‡]
Y_{MKO}	–		16.279 ± 0.024[f]
J_{MKO}	–		15.158 ± 0.013[f]
H_{MKO}	–		14.887 ± 0.021[f]
K_{MKO}	–		14.930 ± 0.020[f]
W_1	8.333 ± 0.023[j]		14.204 ± 0.123[f, j]
W_2	8.127 ± 0.020[j]		13.430 ± 0.128[f, j]
W_3	7.982 ± 0.021[j]		–
W_4	8.004 ± 0.229[j]		–
F_{NUV}/F_J	7.1×10^{-5}[a, f, g]		–
F_{FUV}/F_J	$<2.2 \times 10^{-5}$[f,g,#]		–
F_X/F_J	5.7×10^{-3}[a, f, h]		–
Mass (M$_\odot$)	0.26 ± 0.06[i]	0.09 ± 0.03[i]	0.068 ± 0.007[f]
Age	1–1.0 Gyr[f]		

Notes. [a]2MASS position, epoch 1998.811 Skrutskie et al. (2006).
[b]Epoch 2012.90 Janson et al. (2014).
[c]spectrum of combined object Riaz et al. (2006).
[d]based on flux ratio Janson et al. (2012).
[e]Lépine & Gaidos (2011).
[f]this work.
[g]Janson et al. (2012).
[h]Voges et al. (2000).
[i]Janson et al. (2014).
[j]Wright et al. (2010).
†2MASS confusion flag set.
‡marked as diffraction spike in 2MASS.
*photometric parallax.
#3σ upper limit.

each exposure. This process results in an astrometric systematic floor of ≈10–20 mas.

The in-database measurement of parallax (0.080 ± 0.010 arcsec) and proper motion does not yet include a robust outlier rejection scheme. All 11 PS1 measurements spanning 3 yr were included in this analysis. We found that a careful assessment of possible outliers, and the impact of the outlier rejection, is necessary to have confidence in the parallax and proper motion fits. While we are working to incorporate these checks in the automatic analysis, we have used an external calculation for 2MASS J0213+3648 C for the purpose of this article.

Figs 4 and 5 show the astrometry of 2MASS J0213+3648 C. We have used bootstrap resampling to determine the errors on the fitted parameters and to assess whether the inclusion of any specific

measurement in the calculation of the fit drives the parameters to significantly different values. For 1000 bootstrap resample tests, we also measured the distance of each point from the fitted path, scaled by the formal error on the point. The median of this distribution is a measure of how deviant the point is from the path, in the given set of measurements. We find that one point, marked with an 'X' on Fig. 4, is significantly deviant from the collection of fitted paths. The mean parallax changes by a substantial amount, though formally the two values are within error. We remove that single discrepant point from the data set and use the resulting parallax and proper motion values for 2MASS J0213+3648 C. Our final Pan-STARRS 1 parallax measurement for 2MASS J0213+3648 C is 0.045 ± 0.010 arcsec, corresponding to a distance of $22.2^{+6.4}_{-4.0}$ pc.
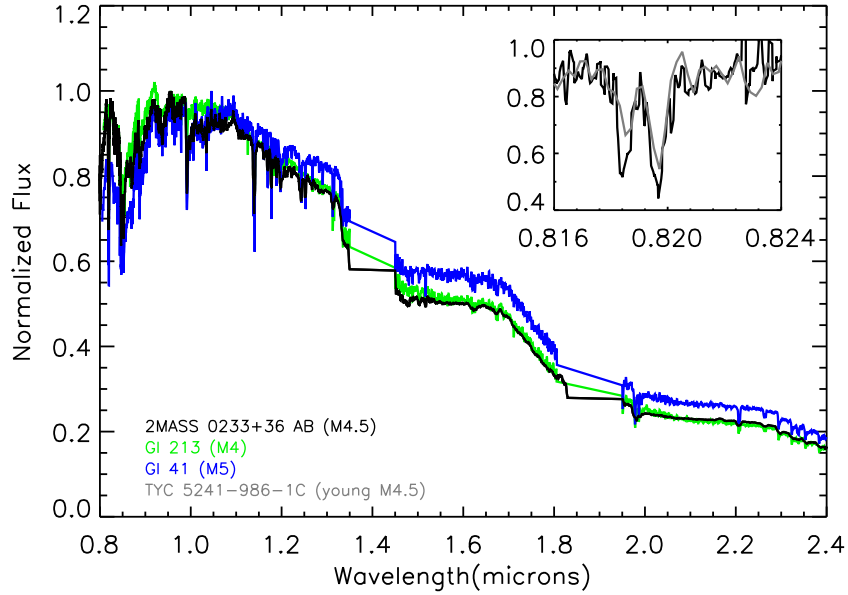
Figure 3. The SpeX/IRTF spectrum of 2MASS J0213+3648 AB. Two comparison spectra of M4 and M5 standards from Kirkpatrick et al. (2010) are shown in the main plot. The spectra are normalized at 0.9 μm. The inset shows the 8200 Å feature compared to the 20 Myr to ∼125 Myr old M4.5 TYC 5241-986-1 C (Deacon et al. 2013).
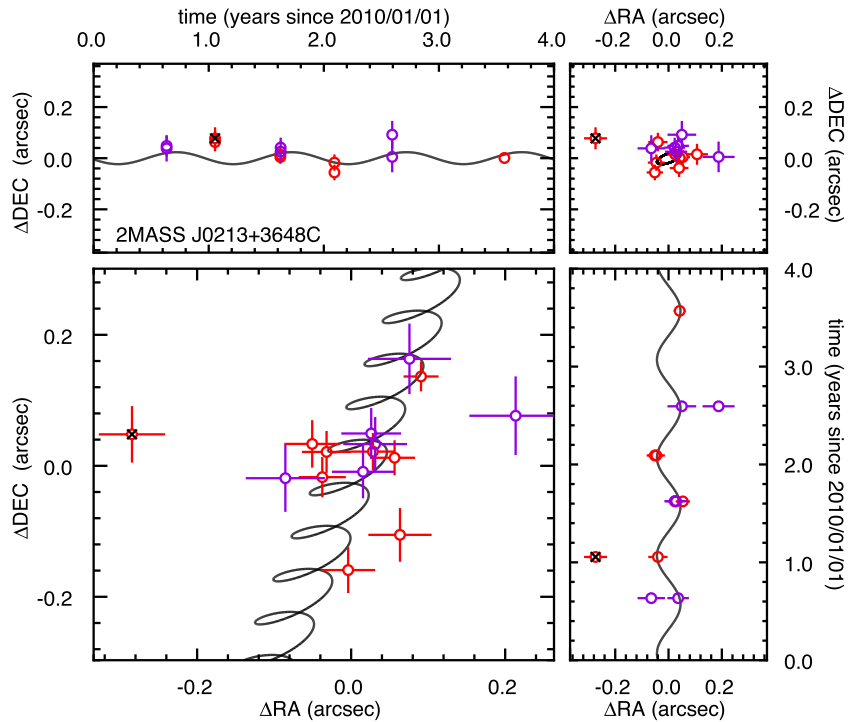

Figure 4. Lower left: the relative positions of the Pan-STARRS 1 z_{P1} (blue) and y_{P1} (red) measurements for 2MASS J0213+3648 C. The best fitted path on the sky is drawn in black. The single point with a black X is suspect and excluded from the final fit. Upper left: Residual Declination positions as a function of time (MJD) after the proper-motion fit has been subtracted; symbols as above. Lower right: same as Upper-left for Right Ascension. Upper right: Residual Declination versus Right Ascension after the proper-motion fit has been subtracted; symbols as above.

2.6 WISE photometry

2MASS J0213+3648 C does not appear in the AllWISE catalogue or reject table, likely due to its bright primary. To remove the primary and hence estimate the brightness of the C component, we modelled the Point Spread Function (PSF) of the primary on the downloaded WISE images. Lang, Hogg & Schlegel (2014) mod-

elled the WISE PSF as three isotropic Gaussians. We found that two bivariate Gaussians with free axial tilts were a better fit to our primary. The PSF was fitted to the central 10 pixels of the primary to exclude any flux from the secondary. We then subtracted the approximated PSF from the full image revealing the tertiary in better contrast. See Fig. 6 for the results of this subtraction. Finally, we undertook aperture photometry on the tertiary component using two
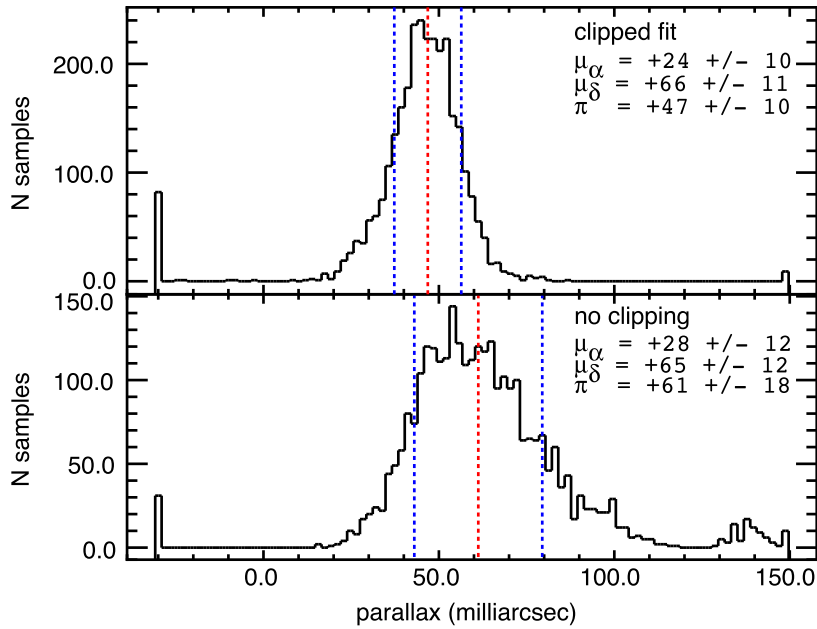
Figure 5. Bootstrap resampling tests of the astrometric errors. Top: histogram of the fitted parallax values for 3000 bootstrap resampling tests, with all points included. The blue dashed line marks the 50 per cent point in the cumulative distribution function. The red dashed lines represent the 15.9 per cent and 84.1 per cent points, equivalent to $\pm 1\sigma$. The fitted parallax and proper motion values are listed with the errors derived from this analysis. Bottom: histogram of the fitted parallax values for 3000 bootstrap resampling tests, with the single outlier point excluded. Labels as above.
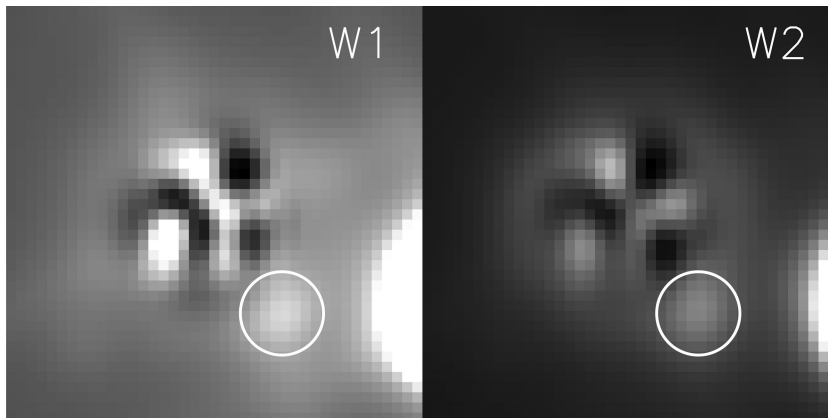
Figure 6. The results of our WISE PSF subtraction with 2MASS J0213+3648 C circled. These images are 55 arcsec across.

apertures on either side of the object but at similar distances from the primary to measure the background flux. We then used the same technique on other stars in the field and compared the measured fluxes to the WISE catalogue magnitudes in order to determine the image zeropoints. We found that 2MASS J0213+3648 C had $W_1 = 14.204 \pm 0.123$ mag and $W_2 = 13.430 \pm 0.128$ mag.

3 RESULTS

The derived properties of the components of the 2MASS J0213+3648 system are shown in Table 1. Below we discuss how these parameters were calculated.

3.1 Properties of 2MASS J0213+3648 AB

2MASS J0213+3648 was identified as an M dwarf in the solar neighbourhood with significant X-ray emission by Riaz et al. (2006). Using low-resolution spectroscopy, they classified it as

an M4.5 dwarf [a spectral type confirmed by Alonso-Floriano et al. (2015)] with a spectrophotometric distance of 11 pc. Riaz et al. (2006) also reported that the object showed Hα emission of 8.1 Å. Janson et al. (2012) used Lucky Imaging to identify 2MASS J0213+3648 A as a close binary system with a separation of 0.181 ± 0.002 arcsec and an estimated orbital period of 8 yr. We note here that this orbital period is too long for either component of the binary to have its activity significantly affected by tidal spin-up. The subsequent orbital motion combined with the component's flux ratio led Janson et al. (2014) to estimate spectral types of M4.5 and M6.5 and masses of 0.26 ± 0.06 M$_\odot$ and 0.09 ± 0.03 M$_\odot$ for the A and B components, respectively.

3.1.1 The age of 2MASS J0213+3648 AB

The primary pair has an X-ray counterpart in the *ROSAT* Bright Source Catalogue (Voges et al. 1999) 13 arcsec away, slightly beyond the 1σ positional error of 11 arcsec. We estimated the

X-ray flux for 2MASS J0213+3648 AB by applying the relations of Schmitt, Fleming & Giampapa ([1995](#)) to the *ROSAT* data yielding a flux of $5.2 \pm 1.4 \times 10^{-13}$ ergs cm^{-2}. We then used 2MASS *J*-band magnitude of 2MASS J0213+3648 AB to calculate an F_X/F_J flux ratio of 5.7×10^{-3}. Comparing this value to fig. 3 of Shkolnik, Liu & Reid ([2009](#)), we first note that our target is bluer in $I - J$ than one would expect for an M4.5 (using an *I* magnitude from SuperCOSMOS; Hambly et al. [2001](#)). However, this does not affect the conclusion that the object lies on the active M dwarf sequence. This sequence is defined as having similar or greater X-ray emission than the Pleiades (125 Myr; Stauffer, Schultz & Kirkpatrick [1998](#)) and the β Pictoris young moving group (21 Myr; Binks & Jeffries [2013](#)). We note that 2MASS J0213+3648 AB also emits a higher X-ray flux than most Hyades (625 Myr; Perryman et al. [1998](#)) members of a similar spectral type. Riaz et al. ([2006](#)) find $\log_{10} L_X/L_{bol} = 3.16$, placing it in their saturated X-ray emission locus. Comparing this value with fig. 5 of Preibisch & Feigelson ([2005](#)), we find that 2MASS J0213+3648 AB fractional X-ray flux is similar to, if not higher than, Hyades M dwarf members and much higher than the vast majority of field M dwarfs. Using the method of Malo et al. ([2014](#)), we calculated that 2MASS J0213+3648 A/B has $\log L_x = 28.5 \pm 0.6$ ergs s^{-1}. This is 2σ less active than the β Pictoris moving group and 1σ less active than the AB Dor association. We do, however, find that it is 1.2σ more active than the typical field star of a similar type.

As our object is a binary, it is possible that the X-ray flux is coming entirely from the M6.5 secondary component. This would not alter our conclusion that the object is X-ray active as a recalculation of F_X/F_J would result in the object lying even further above the inactive M dwarf regime on fig. 3 of Shkolnik et al. ([2009](#)). If we were relying solely on X-ray emission for an age diagnostic, we would estimate that this object is younger than the Hyades (i.e. <625 Myr).

2MASS J0213+3648 AB are also detected by the *GALEX* satellite (Martin et al. [2005](#)) in the near-UV band but not in the far-UV band. We note that it does appear as a far-UV emitter in the EUVE catalogue (Christian et al. [1999](#)) due to a stellar flare. The *GALEX* near-UV flux of 20.1 ± 2.4 μJy results in an F_{NUV}/F_J ratio of 7.1×10^{-5} or an F_{NUV}/F_{K_s} ratio of 7.7×10^{-5}. We note that the latter value is within 0.2 dex of the young (20–125 Myr) M4.5 binary TYC 5241-986-1 BC (Deacon et al. [2013](#)). We set an upper limit on the FUV flux of 2MASS J0213+3648 AB by finding the flux error on the forced far-UV photometry at the position of the *GALEX* NUV detection. From this, we calculate a 3σ upper limit of $F_{FUV}/F_J < 2.2 \times 10^{-5}$. To further examine the near-UV properties of 2MASS J0213+3648 AB, we must compare with fig. 3 of Shkolnik et al. ([2011](#)). Here, we find that our object appears to lie between the active and inactive loci and that while it does not have a far-UV detection, it could have emission above Shkolnik et al. ([2009](#))'s $F_{NUV}/F_J > 10^{-5}$ and still remain undetected by *GALEX*. However, the near-UV emission is of little use as Ansdell et al. ([2014](#)) noted that the fully convective transition in mid-M dwarfs makes it impossible to define a near-UV inactive locus of M dwarfs beyond M3. Hence, we do not consider 2MASS J0213+3648 AB's near-UV emission to be a reliable age diagnostic.

Riaz et al. ([2006](#)) found that 2MASS J0213+3648 AB has Hα in emission. West et al. ([2008](#)) provide a list of activity lifetimes as a function of the spectral type. As the activity lifetime changes with the spectral type, we need to know which component this emission comes from. While we were not able to resolve the Hα emission into

two separate components in our CAFE spectrum, we were able to measure its equivalent width as -6.6 Å, broadly in agreement with Riaz et al. ([2006](#))'s value of -8.1 Å and the value of $-6.2^{+0.4}_{-0.2}$ Å from Alonso-Floriano et al. ([2015](#)). This emission could in theory come from either component of the inner binary. Using the mean χ correction factors as a function of the spectral type of Walkowicz, Hawley & West ([2004](#)), we estimated the $\log L_{H\alpha}/L_{bol}$ to be -3.4 (from our EW of -6.6 Å) if the emission was coming from the A component. This is in the most active quartile for stars of a similar spectral type in fig. 6 of Schmidt et al. ([2015](#)) but is not outside the bounds of the activity range in their sample. For the secondary component, we used the *i* band flux ratio of Janson et al. ([2012](#)) and the typical $r - i$ colour difference between an M4.5 and M6.5 in the SED templates of Kraus & Hillenbrand ([2007](#)) to estimate an *r*-band contrast ratio of 2.59. We then used this value to adjust the EW of the Hα feature to take into account the lower continuum in the *r* band for an M6.5. This resulted in an approximate equivalent width of 72 Å if the emission is coming entirely from the secondary. Again using the method of Walkowicz et al. ([2004](#)), we calculated $\log L_{H\alpha}/L_{bol}$ to be -3.0 if all the Hα emission was coming from the secondary component. This is more active than any M6 or M7 in Schmidt et al. ([2015](#))'s fig. 6 (with $\log L_{H\alpha}/L_{bol}$ declining with increasing spectral type). Hence, we conclude that it is unlikely that all the Hα emission is from the secondary component and that the M4.5 A component must be active. However, Morgan et al. ([2012](#)) show that binaries in the 1–100 AU separation range have significantly higher activity fractions. Hence, we cannot use this activity to set an upper age bound.

Young M dwarf stars in star-forming regions typically have infrared excesses caused by circumstellar discs. We used the WISE photometry (Wright et al. [2010](#)) for 2MASS J0213+3648 AB to examine if it has mid-infrared excess indicative of a disc. Comparing with the $W_3 - W_4$ versus $W_1 - W_2$ plot shown in fig. 1 of Simon et al. ([2012](#)), we find that our target falls close to the stellar locus suggesting that our primary does not host a disc. As discussed in Deacon et al. ([2013](#)), discs around M dwarfs are uncommon for ages beyond 20 Myr. While studies of younger (10–15 Myr) clusters show significant amounts of disc emission around many M dwarfs (e.g. Currie et al. [2008](#)), Simon et al. ([2012](#)) found no disc excesses in the M dwarf population of Tucana Horologium (45 ± 4 Myr, Bell, Mamajek & Naylor [2015](#)) and AB Dor (149^{+51}_{-19} Bell et al. [2015](#)). Hence, the lack of disc excess indicates that 2MASS J0213+3648 AB is older than around 20 Myr.

The Na 8200 Å doublet provides an effective gravity diagnostic for mid-late M dwarfs (Lyo, Lawson & Bessell [2004](#); Schlieder et al. [2012](#)). We measured the equivalent width of this feature in our IRTF spectrum and found it to be 5.8 ± 1.8 Å on the upper end of the field dwarf sequence in Schlieder et al. ([2012](#))'s fig. 3. This points towards an older lower age boundary of $\sim$1 Gyr. A visual comparison with the young (20–125 Myr) M4.5 TYC 5241-986-1 B/C (Deacon et al. [2013](#)) also indicates that 2MASS J0213+3648 AB is not a young object (see Fig. [3](#) inset). We also used the NaI spectral index derived by Lyo et al. ([2004](#)) and measured a value of 1.25 ± 0.15. Fig. [7](#) shows that our object has a feature strength (and thus a gravity) consistent with field dwarfs. While the M6.5 component will have a deeper 8200 Å doublet owing to its late spectral type, the contrast ratio of $\Delta i = 2.16 \pm 0.15$ mag indicates that it will contribute less than 10 per cent of the flux in this region and thus will not significantly change the line depth. This NaI spectral index value has a relatively high error due to low S/N in the surrounding continuum region. Both the visual comparison of the 8200 Å feature and the lack of other youth indicators suggest that
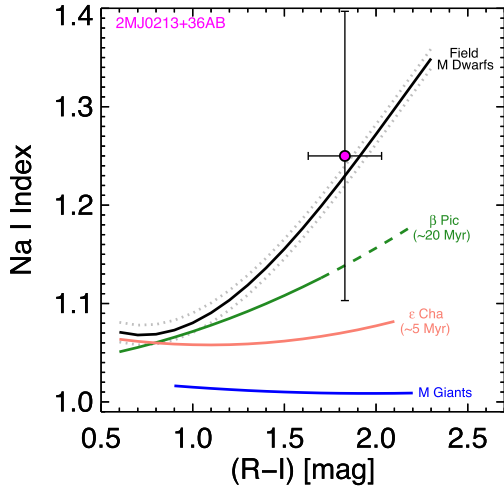
Figure 7. The Na I index from Lyo et al. (2004) along with the measured sequences for different populations from Lawson, Lyo & Bessell (2009). 2MASS J0213+3648 lies just above the old field sequence.

this is not a young object. Additionally, we found that the strength of TiO (TiO5 0.436, M3.7; TiO6 0.66, M4.0), CaH (CaH3 0.61, M5.6), VO (VO1 0.90, M5.4; VO2 0.72, M4.9) and H_2O (H2OD 1.14) molecular indices in the optical (Lépine et al. 2013) and near-infrared (McLean et al. 2003; Allers & Liu 2013) absorption features of 2MASS J0213+3648 A/B is consistent with a spectral type of M5.0 ± 0.5. This is in agreement with the literature spectral type of M4.5 (Riaz et al. 2006).

One final youth indicator available to us is kinematics. We ran 2MASS J0213+3648 AB through the BANYAN II online tool (Malo et al. 2013; Gagné et al. 2014) and found that its kinematics do not match any of the known young moving groups. We also plotted our object on a series of diagnostic plots comparing its Galactic XYZ positions and UVW space velocities (Fig. 8). Again, we find that 2MASS J0213+3648 AB does not match any known young moving groups and lies outside the loosely defined young ($\lesssim 125$ Myr) Local Association (Zuckerman & Song 2004). We also found that 2MASS J0213+3648 AB did not match the kinematics of other groups not shown in our plot: Octans (Murphy & Lawson 2014), Hercules-Lyra (Eisenbeiss et al. 2013), 32 Ori (Mamajek 2006), Carina Near (Zuckerman et al. 2006) and Ursa Majoris (King et al. 2003).

In summary, we assign an upper age bound of 10 Gyr for 2MASS J0213+3648 AB based on disc kinematics and a lower age boundary of 1 Gyr based on the strength of the Na 8200 Å feature. We note that 2MASS J0213+3648 AB has X-ray emission indicative of it being younger than the Hyades. However, we caution that the relatively late spectral type of this object and its multiplicity make it difficult to apply some age diagnostics such as UV emission with sufficient certainty.

3.2 Properties of 2MASS J0213+3648 C

The observed near-infrared spectrum of 2MASS J0213+3648 C is shown in Fig. 9. We spectrally classified 2MASS J0213+3648 C using the flux indices of Burgasser et al. (2006) and the polynomial relations of Burgasser (2007). The individual indices and the derived spectral types are shown in Table 2. We also compared visually with the standards of Burgasser et al. (2006), finding a best fit of T3 [note the T3 standard of Burgasser et al. (2006)] was found

to be a binary by Liu, Dupuy & Leggett (2010), see later discussion on the comparison with the newer standard). As this compares well with the spectral types derived from the indices, we adopt this as our final spectral type. Fig. 9 also shows a comparison with the young (~100 Myr) T3 GU Psc b (Naud et al. 2014), the young (~300 Myr) T2.5 HN Peg B (Luhman et al. 2007), the original T3 standard (2MASS J120956.13−100400.8, Burgasser et al. 2006), and the alternative T3 standard (SDSS J120602.51+281328.7) suggested by Liu et al. (2010) after 2MASS J120956.13−100400.8 was found to be a binary. We note that 2MASS J0213+3648 C has a narrower *J* band peak and deeper *J*-band water absorption than SDSS J120602.51+281328.7 but matches both HN Peg B and 2MASS J120956.13−100400.8 well in this regime, the *H* and *K* bands the spectrum are a better fit to SDSS J120602.51+281328.7. GU Psc b is unique amongst our comparison objects in that it shows a distinct slope in the *Y* and *J* bands compared to the other objects. We do not see sufficient evidence to suggest that 2MASS J0213+3648 C is spectrally peculiar and note that it does not have the enhanced *K*-band emission that Naud et al. (2014) attributed to reduced collision-induced absorption resulting from the lower surface gravity (i.e. younger age) of GU Psc b. 2MASS J0213+3648 C is the only known T3 benchmark companion known (see Fig. 10). Our measured WISE photometry yields $W_1 - W_2 = 0.77$, in line with the expect colour for an early-mid T dwarf (Kirkpatrick et al. 2011).

To compare with our trigonometric parallax measurement from Pan-STARRS 1, we calculated a photometric distance for 2MASS J0213+3648 C using only our WFCAM photometry. This was done in a similar manner to Deacon et al. (2014) using the relations of Dupuy & Liu (2012) by calculating distances in each band along with the error on these distances caused by the photometric measurement error and the error in spectral type. We then used the quadrature sum of these error terms to estimate a distance based on the *J*, *H*, and *K* bands. Our final distance is $15.08^{+3.0}_{-2.5}$ pc, which includes both the calculated error due to photometric and spectroscopic measurement uncertainty and the scatter around the absolute magnitude relations. It compares well with the photometric distance of the AB component $14.7^{+6.2}_{-3.3}$ pc (Lépine & Gaidos 2011) and the parallactic distance of $22.2^{+6.3}_{-4.0}$ pc.

3.2.1 Comparison with evolutionary models

We calculated the bolometric correction for 2MASS J0213+3648 C using the polynomial relations of Liu et al. (2010). This resulted in an MKO *J*-band correction of $BC_J = 2.24 \pm 0.14$. We combined this with our WFCAM observations to yield an apparent bolometric magnitude of 17.40 ± 0.50 mag (including the error in our parallax measurements). To determine the physical properties of 2MASS J0213+3648 C, we ran a Monte Carlo comparison to the Baraffe et al. (2003) evolutionary models. For each realisation we randomly drew an age for the system from a flat distribution with between our upper and lower age boundaries (10 Gyr and 1 Gyr), and the apparent bolometric magnitude and parallax were both offset by a random Gaussian offset with a standard deviation equal to the measurement errors. This resulted in an age and absolute bolometric magnitude for each realization. The mass, effective temperature and gravity corresponding to that absolute bolometric magnitude and age were then determined from the Baraffe et al. (2003) model grid. The results are shown in Fig. 11 with values of $T_{\rm eff} = 1641 \pm 167$ K, $m = 68 \pm 7 M_J$ and $\log g = 5.45 \pm 0.08$ dex (cgs). Note that this relatively high temperature (for a T3) is likely due to our distance from the trigonometric parallax being larger than our photometric distance.
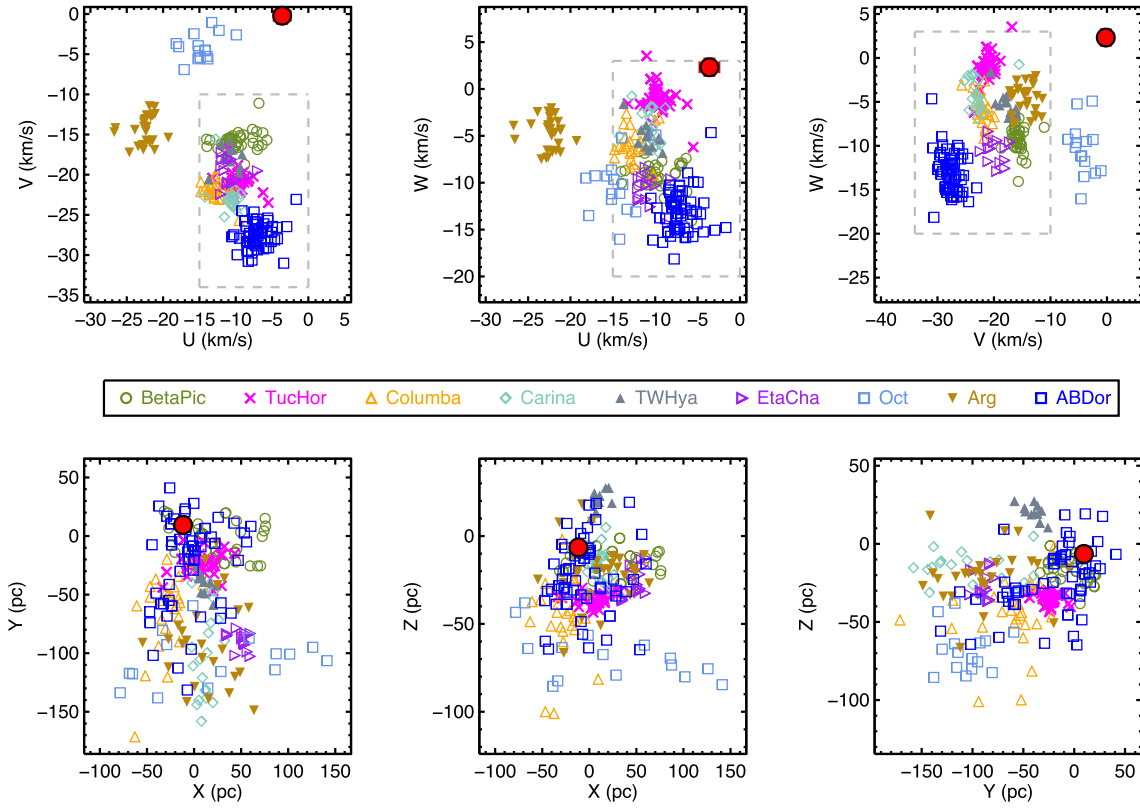
Figure 8. A plot showing the positions of known young moving groups and our target system 2MASS J0213+3648 (red circle). The dotted box shows the broadly young Local Association (Zuckerman & Song 2004).
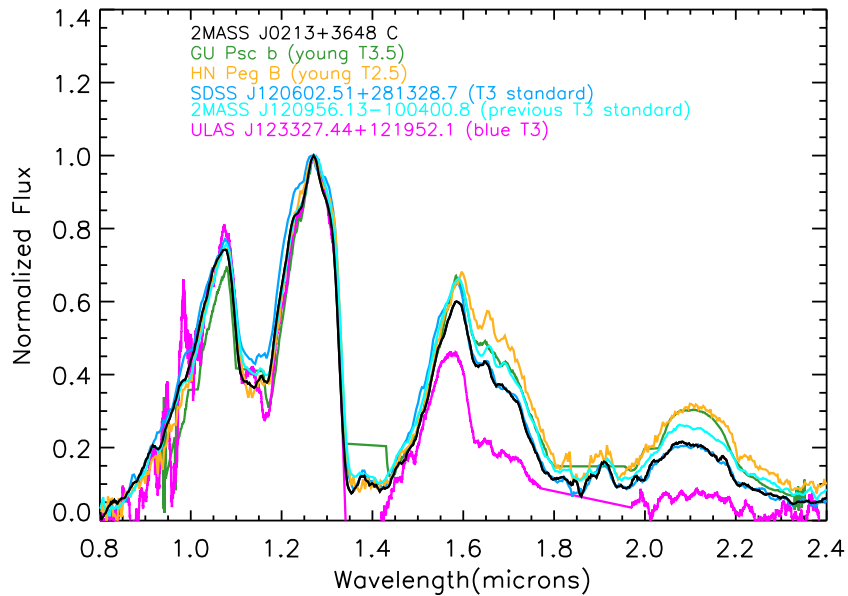
Figure 9. Our spectrum of 2MASS J02132062+3648506C, we classify this object as a T3 ± 0.5. Shown for comparison are the spectra for the young (∼100 Myr) T3.5 GU Psc b (Naud et al. 2014), the young (∼300 Myr) T2.5 HN Peg B (Luhman et al. 2007), the alternative T3 dwarf standard SDSSJ120602.51+281328.7 (Chiu et al. 2006) [as suggested by Liu et al. (2010)], the previous T3 standard 2MASS J120956.13−100400.8 (Burgasser et al. 2004, 2006; now known to be a binary) and the blue T dwarf (Burningham et al. 2010; Marocco et al. 2015). All spectra are smoothed to similar resolutions and normalized to the *J*-band peak.

3.2.2 The absolute magnitude of 2MASS J0213+3648 C

We calculated absolute magnitudes in the MKO system based on both our trigonometric parallax for the tertiary component and the Lépine & Gaidos (2011) photometric parallax for the unresolved inner pair. These are for the trigonometric parallax $M_J = 13.424 \pm 0.483$ mag, $M_H = 13.153 \pm 0.483$ mag and $M_K = 13.196 \pm 0.483$ mag and $M_J = 14.321 \pm 0.639$ mag,

Table 2. Spectral classification of 2MASS J0213+3648 C. Shown are the spectral indices (Burgasser et al. 2006) and the implied spectral classifications from polynomial relations (Burgasser 2007) for each index.

H$_2$O-J (SpT)	CH$_4$-J (SpT)	H$_2$O-H (SpT)	CH$_4$-H (SpT)	CH$_4$-K (SpT)	Visual Type	Final Type
0.395 ± 0.013 (T3.7)	0.450 ± 0.019 (T4.3)	0.435 ± 0.026 (T3.7)	0.709 ± 0.027 (T2.5)	0.432 ± 0.034 (T3.1)	T3	T3
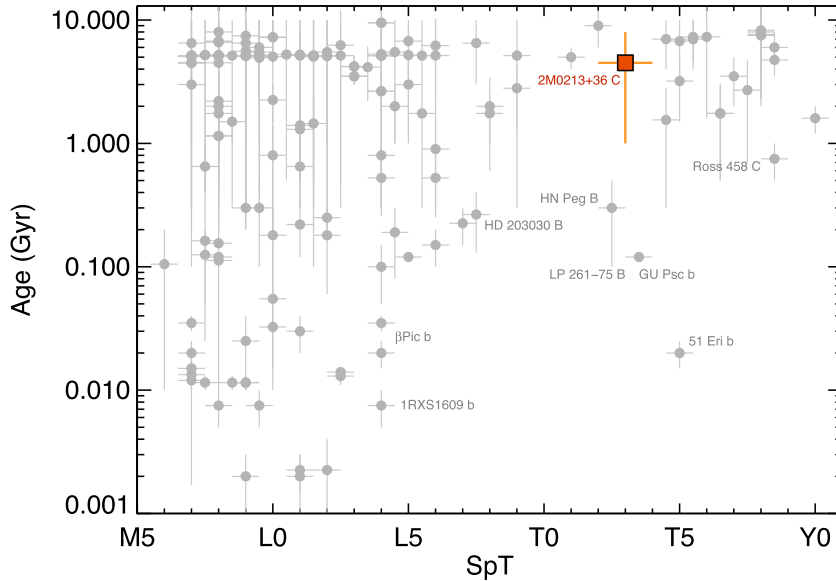
Figure 10. An updated version of the benchmark companion age-spectral type plot from Bowler et al. (2015). The data for this plot come largely from the compilation of Deacon et al. (2014). 2MASS J0213+3648 C adds a field-age early-mid T benchmark into an area of the diagram, which was previously sparsely populated.

$M_H = 14.050 \pm 0.639$ mag and $M_K = 14.093 \pm 0.639$ mag with the error estimates dominated by the uncertainties on the distance measurements. Comparing with the absolute magnitude to the spectral type plots of fig. 27 of Dupuy & Liu (2012), we find that the absolute magnitudes calculated with the photometric parallax lie on the main locus of early T dwarfs. The absolute magnitudes based on the trigonometric parallax are approximately one magnitude over-luminous or approximately 2σ. This suggests that either the trigonometric parallax is a chance underestimate or perhaps that the secondary is over-luminous due to binarity. Both of these explanations would also fit our anomalously hot effective temperature estimate from evolutionary models.

3.2.3 Comparison with atmospheric models

Atmospheric models provide an independent way to infer the physical properties of 2MASS J0213+3648 C. We fit the solar metallicity BT-Settl-2010 grid of synthetic spectra (Allard, Homeier & Freytag 2011) spanning 500–1500 K in effective temperature and 4.0–5.5 dex in surface gravity (log g [cgs]) to our prism spectrum, flux-calibrated to our UKIRT J-band photometry. The 1.60–1.65 μm region is ignored in the fits owing to poorly calibrated methane opacities in this region of the models. The 1.80–1.95 μm region is also excluded because telluric absorption is particularly strong and difficult to accurately correct in this region. The fitting procedure follows a maximum likelihood approach as described in detail in Bowler et al. (2011). In brief, we calculate reduced χ^2 values for each model in 100 K increments in $T_{\rm eff}$ and 0.5 dex in log g. The multiplicative factor to scale the model to the flux-calibrated

spectrum corresponds to the ratio of the object's radius to its distance, squared. Adopting the astrometric distance of 22 pc yields a corresponding radius for each synthetic spectrum. The best fitting model has $T_{\rm eff} = 1300$ K, log $g = 5.0$ dex and a radius of 1.1 $R_{\rm Jup}$ (Fig. 12). This model does not reproduce our spectrum very well, however, particularly in the 1.0–1.3 μm range. Systematic errors of several hundred Kelvin are not uncommon when fitting model atmospheres to brown dwarf spectra as a result of incomplete line lists, missing sources of opacity, and non-solar chemical abundances (e.g. Deacon et al. 2012b).

4 CONCLUSIONS

We have discovered a wide T3 companion to the M4.5+M6.5 binary 2MASS J02132062+3648506. T dwarfs in higher order multiple systems are relatively rare, this being the fifth such system discovered after Gl 570 D (Burgasser et al. 2000),Wolf 1130 B (Mace et al. 2013), Ross 458 C (Goldman et al. 2010) and ξ UMa E (Wright et al. 2013). The central binary of 2MASS J0213+3648 has Hα and X-ray activity along with UV flaring, suggesting that it may be young (with the X-ray emission pointing towards it being younger than the Hyades). However, its strong Na 8200 Å absorption and kinematics inconsistent with known young moving groups means we adopt a conservative age range of 1–10 Gyr. This means that 2MASS J02132062+3648506C provides an older equivalent to the young, similar spectral-type benchmarks GU Psc b (Naud et al. 2014) and HN Peg B (Luhman et al. 2007). Fig. 10 shows how our object fills a previous gap in field-age early-mid T benchmark systems.
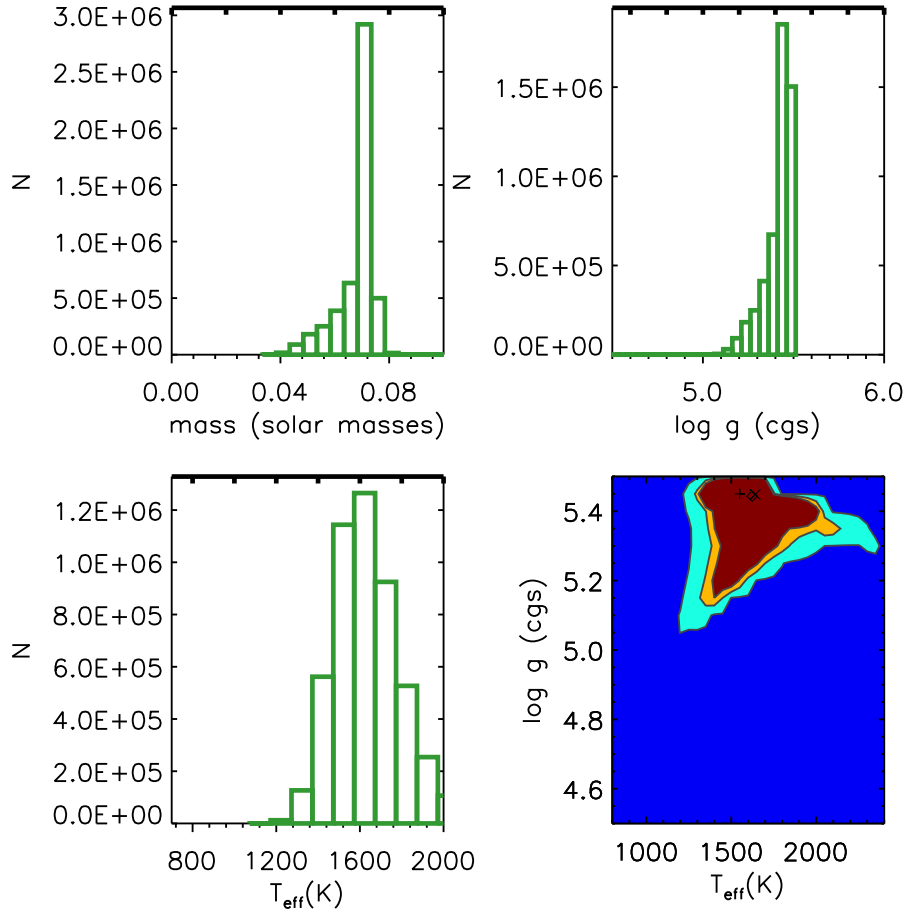
Figure 11. Evolutionary model predictions for 2MASS J0213+3648 C assuming a flat age range of 1–10 Gyr. The results of 5000 000 Monte Carlo realizations of the object and comparison with the Baraffe et al. (2003). The + symbol in the bottom right panel marks the mean T_{eff} and $\log g$ predicted by the comparison and the diamond marks the median values while the cyan, yellow and maroon regions show the 3σ, 2σ, and 1σ confidence regions, respectively.
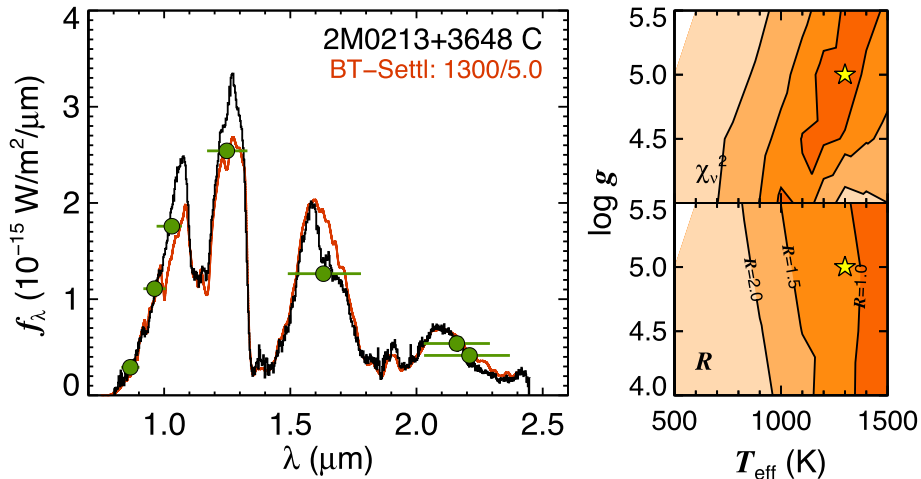
Figure 12. The result of our comparison between our spectrum for 2MASS J0213+3648 C and the BT-Settl models (Allard et al. 2011). The green points in the left-hand panel show our Y, J, H and K UKIRT photometry and the 2MASS K_S photometry. The right-hand panel shows the likelihood contours for the different parameters with the most probable values marked with a star.

ACKNOWLEDGEMENTS

REFERENCES

Aceituno J. et al., 2013, A&A, 552, A31

Allard F., Homeier D., Freytag B., 2011, in Johns-Krull C. M., Browning M. K., West A. A., eds, ASP Conf. Ser. Vol. 448, 16th Cambridge Work. Cool Stars. Stellar Syst. Sun, Astron. Soc. Pac., San Francisco, p. 91

Allen P. R., Burgasser A. J., Faherty J. K., Kirkpatrick J. D., 2012, AJ, 144, 62

Allers K. N., Liu M. C., 2013, ApJ, 772, 79

Alonso-Floriano F. J. et al., 2015, A&A, 577, A128

Ansdell M. et al., 2014, ApJ, 798, 41

Baraffe I., Chabrier G., Barman T. S., Allard F., Hauschildt P. H., 2003, A&A, 712, 701

Bell C. P. M., Mamajek E. E., Naylor T., 2015, MNRAS, 454, 593

Best W. M. J. et al., 2013, ApJ, 777, 84

Best W. M. J. et al., 2015, ApJ, 814, 118

Binks A. S., Jeffries R. D., 2013, MNRAS, 438, L11

Bowler B. P., Liu M. C., Kraus A. L., Mann A. W., Ireland M. J., 2011, ApJ, 743, 148

Bowler B. P. et al., 2015, ApJ, 806, 62

Burgasser A. J., 2007, ApJ, 659, 655

Burgasser A. J. et al., 2000, ApJ, 531, L57

Burgasser A. J., McElwain M. W., Kirkpatrick J. D., Cruz K. L., Tinney C. G., Reid I. N., 2004, AJ, 127, 2856

Burgasser A. J., Kirkpatrick J. D., Lowrance P. J., 2005, AJ, 129, 2849

Burgasser A. J., Geballe T. R., Leggett S. K., Kirkpatrick J. D., Golimowski D. A., 2006, ApJ, 637, 1067

Burningham B. et al., 2010, MNRAS, 406, 1885

Casali M. et al., 2007, A&A, 467, 777

Chambers K. C. et al., 2016, preprint (arXiv:1612.05560)

Chiu K., Fan X., Leggett S. K., Golimowski D. A., Zheng W., Geballe T. R., Schneider D. P., Brinkmann J., 2006, AJ, 131, 2722

Christian D. J., Craig N., Cahill W., Roberts B., Malina R. F., 1999, AJ, 117, 2466

Crepp J. R. et al., 2012, ApJ, 751, 97

Currie T., Kenyon S. J., Balog Z., Rieke G., Bragg A., Bromley B., 2008, ApJ, 672, 558

Cushing M. C., Vacca W. D., Rayner J. T., 2004, Publ. Astron. Soc. Pacific, 116, 362

Cutri R. M. et al., 2013, Explanatory Supplement to the AllWISE Data Release Products. Available at: http://wise2.ipac.caltech.edu/docs/release/allwise/expsup/index.html

Deacon N. R. et al., 2011, AJ, 142, 77

Deacon N. R. et al., 2012a, ApJ, 757, 100

Deacon N. R. et al., 2012b, ApJ, 755, 94

Deacon N. R., Schlieder J. E., Olofsson J., Johnston K. G., Henning T., 2013, MNRAS, 434, 1117

Deacon N. R. et al., 2014, ApJ, 792, 119

Delgado-Donate E. J., Clarke C. J., Bate M. R., Hodgkin S. T., 2004, MNRAS, 351, 617

Dupuy T. J., Liu M. C., 2012, ApJS, 201, 19

Dupuy T. J., Liu M. C., Ireland M. J., 2009, ApJ, 692, 729

Dupuy T. J., Liu M. C., Ireland M. J., 2014, ApJ, 790, 133

Eisenbeiss T., Ammler-von Eiff M., Roell T., Mugrauer M., Adam C., Neuhäuser R., Schmidt T. O. B., Bedalov A., 2013, A&A, 556, A53

Faherty J. K., Burgasser A. J., West A. A., Bochanski J. J., Cruz K. L., Shara M. M., Walter F. M., 2010, AJ, 139, 176

Gagné J., Lafrenière D., Doyon R., Malo L., Artigau É., 2014, ApJ, 783, 121

Goldman B., Marsat S., Henning T., Clemens C., Greiner J., 2010, MNRAS, 405, 1140

Hambly N. et al., 2001, MNRAS, 326, 1279

Hodgkin S. T., Irwin M. J., Hewett P. C., Warren S. J., 2009, MNRAS, 394, 675

Irwin M. J. et al., 2004, in Quinn P. J., Bridger A., eds, Proc. SPIE Conf. Ser. Vol. 5493, Optimizing Scientific Return for Astronomy through Information Technologies. SPIE, Bellingham, p. 411

Janson M., Carson J. C., Lafrenière D., Spiegel D. S., Bent J. R., Wong P., 2012, ApJ, 747, 116

Janson M., Bergfors C., Brandner W., Kudryavtseva N., Hormuth F., Hippler S., Henning T., 2014, ApJ, 789, 102

Kaiser N. et al., 2002, in Tyson J. A., Wolff S., eds, Proc. SPIE Conf. Ser. Vol. 4836, Survey and Other Telescope Technologies and Discoveries. SPIE, Bellingham, p. 154

King J. R., Villarreal A. R., Soderblom D. R., Gulliver A. F., Adelman S. J., 2003, AJ, 125, 1980

Kirkpatrick J. D. et al., 2010, ApJS, 190, 100

Kirkpatrick J. D. et al., 2011, ApJS, 197, 19

Kouwenhoven M. B. N., Goodwin S. P., Parker R. J., Davies M. B., Malmberg D., Kroupa P., 2010, MNRAS, 404, 1835

Kraus A. L., Hillenbrand L. A., 2007, AJ, 136, 2340

Lang D., Hogg D. W., Schlegel D. J., 2014, preprint (arXiv:1410.7397)

Law N. M., Dhital S., Kraus A., Stassun K. G., West A. A., 2010, ApJ, 720, 1727

Lawson W. A., Lyo A.-R., Bessell M. S., 2009, MNRAS, 400, L29

Lépine S., Bongiorno B., 2007, AJ, 133, 889

Lépine S., Gaidos E., 2011, AJ, 142, 138

Lépine S., Hilton E. J., Mann A. W., Wilde M., Rojas-Ayala B., Cruz K. L., Gaidos E., 2013, AJ, 145, 102

Liu M. C., Dupuy T. J., Ireland M. J., 2008, ApJ, 689, 436

Liu M. C., Dupuy T. J., Leggett S. K., 2010, ApJ, 722, 311

Liu M. C. et al., 2011, ApJ, 740, L32

Liu M. C. et al., 2013, ApJ, 777, L20

Lodieu N., Pérez-Garrido A., Béjar V. J. S., Gauza B., Ruiz M. T., Rebolo R., Pinfield D. J., Martín E. L., 2014, A&A, 569, A120

Luhman K. L. et al., 2007, ApJ, 654, 570

Lyo A.-R., Lawson W. A., Bessell M. S., 2004, MNRAS, 355, 363

Mace G. N. et al., 2013, ApJ, 777, 36

Magnier E. A., 2006, in Ryan S., ed., Adv. Maui Opt. Sp. Surveill. Technol. Conf., The Maui Economic Development Board, Wailea, Maui, Hawaii, p. E50

Magnier E. A., 2007, in Sterken C., ed., ASP Conf. Ser. Vol. 364, The Future of Photometric, Spectrophotometric, and Polarimetric Standardization. Astron. Soc. Pac., San Francisco, p. 153

Magnier E. A. et al., 2013, ApJS, 205, 20

Magnier E. A. et al., 2016, preprint (arXiv:1612.05240)

Malo L., Doyon R., Lafrenière D., Artigau É., Gagné J., Baron F., Riedel A., 2013, ApJ, 762, 88

Malo L., Artigau É., Doyon R., Lafrenière D., Albert L., Gagné J., 2014, ApJ, 788, 81

Mamajek E. E., 2006, Proc. IAU Vol 2, p. 442

Marocco F. et al., 2015, MNRAS, 449, 3651

Martin D. C. et al., 2005, ApJ, 619, L1

McLean I. S., McGovern M. R., Burgasser A. J., Kirkpatrick J. D., Prato L., Kim S. S., 2003, ApJ, 596, 561

Morgan D. P., West A. A., Garcés A., Catalán S., Dhital S., Fuchs M., Silvestri N. M., 2012, AJ, 144, 93

Murphy S. J., Lawson W. A., 2014, MNRAS, 447, 1267

Naud M.-E. et al., 2014, ApJ, 787, 5

Nidever D. L., Marcy G. W., Butler R. P., Fischer D. A., Vogt S. S., 2002, ApJS, 141, 503

Perryman M. A. C. et al., 1998, A&A, 331, 81

Preibisch T., Feigelson E. D., 2005, ApJS, 160, 390

Raghavan D. et al., 2010, ApJS, 190, 1

Rayner J. T., Toomey D. W., Onaka P. M., Denault A. J., Stahlberger W. E., Vacca W. D., Cushing M. C., Wang S., 2003, PASP, 115, 362

Reipurth B., Mikkola S., 2012, Nature, 492, 221

Riaz B., Gizis J. E., Harvin J., 2006, AJ, 132, 866

Schlafly E. F. et al., 2012, ApJ, 756, 158

Schlieder J. E., Lépine S., Rice E., Simon M., Fielding D., Tomasino R., 2012, AJ, 143, 114

Schmidt S. J., Hawley S. L., West A. A., Bochanski J. J., Davenport J. R. A., Ge J., Schneider D. P., 2015, AJ, 149, 158

Schmitt J. H. M. M., Fleming T. A., Giampapa M. S., 1995, ApJ, 450, 392

Shkolnik E., Liu M. C., Reid I. N., 2009, ApJ, 699, 649

Shkolnik E. L., Liu M. C., Reid I. N., Dupuy T., Weinberger A. J., 2011, ApJ, 727, 6

Simon M., Schlieder J. E., Constantin A.-M., Silverstein M., 2012, ApJ, 751, 114

Skrutskie M. F. et al., 2006, AJ, 131, 1163

Stauffer J. R., Schultz G., Kirkpatrick J. D., 1998, ApJ, 499, L199

Taylor M., 2005, in Shopbell P., Britton M., Ebert R., eds, ASP Conf. Ser. Vol. 347, Astronomical Data Analysis Software and Systems XIV. Astron. Soc. Pac., San Francisco, p. 29

Tonry J. L. et al., 2012, ApJ, 750, 99

Umbreit S., Burkert A., Henning T., Mikkola S., Spurzem R., 2005, ApJ, 623, 940

Vacca W. D., Cushing M. C., Rayner J. T., 2003, PASP, 115, 389

Voges W. et al., 1999, A&A, 349, 389

Voges W. et al., 2000, IAU Circ, 7432, 3

Walkowicz L. M., Hawley S. L., West A. A., 2004, PASP, 116, 1105

West A. A., Hawley S. L., Bochanski J. J., Covey K. R., Reid I. N., Dhital S., Hilton E. J., Masuda M., 2008, AJ, 135, 785

Wright E. L. et al., 2010, AJ, 140, 1868

Wright E. L. et al., 2013, AJ, 145, 84

Zuckerman B., Song I., 2004, ARA&A, 42, 685

Zuckerman B., Bessell M. S., Song I., Kim S., 2006, ApJ, 649, L115

This paper has been typeset from a TEX/LATEX file prepared by the author.